Front. Chem. Sci. Eng. 2020, 14(6): 956–966
https://doi.org/10.1007/s11705-019-1907-z

RESEARCH ARTICLE

Efficient degradation of orange II by $ZnMn_2O_4$ in a novel photo-chemical catalysis system

Qingzhuo Ni[1,2,3], Hao Cheng[2], Jianfeng Ma (✉)[1,2], Yong Kong[1], Sridhar Komarneni (✉)[4]

1 School of Environmental and Safety Engineering, Changzhou University, Changzhou 213164, China
2 Guangxi Key Laboratory of Green Processing of Sugar Resources, College of Biological and Chemical Engineering, Guangxi Science University of and Technology, Liuzhou 545006, China
3 Jiangsu Key Laboratory of Oil-Gas Storage and Transportation Technology, Changzhou University, Changzhou 213164, China
4 Department of Ecosystem Science and Management and Materials Research Institute, The Pennsylvania State University, University Park, PA 16802, USA

Abstract A $ZnMn_2O_4$ catalyst has been synthesized via a sucrose-aided combustion method and characterized by various analytical techniques. It is composed of numerous nanoparticles (15–110 nm) assembled into a porous structure with a specific surface area (SSA) of 19.1 $m^2 \cdot g^{-1}$. Its catalytic activity has been investigated for the degradation of orange II dye using three different systems, i.e., the photocatalysis system with visible light, the chemocatalysis system with bisulfite, and the photo-chemical catalysis system with both visible light and bisulfite. The last system exhibits the maximum degradation efficiency of 90%, much higher than the photocatalysis system (15%) and the chemocatalysis system (67%). The recycling experiments indicate that the $ZnMn_2O_4$ catalyst has high stability and reusability and is thus a green and eximious catalyst. Furthermore, the potential degradation mechanisms applicable to the three systems are discussed with relevant theoretical analysis and scavenging experiments for radicals. The active species such as Mn(III), $O_2^{\bullet-}$, h^+, e_{aq}^-, $SO_4^{\bullet-}$ and $HO^{\bullet}$ are proposed to be responsible for the excellent degradation results in the photo-chemical catalysis system with the $ZnMn_2O_4$ catalyst.

Keywords $ZnMn_2O_4$, photo-chemical catalysis, bisulfite, dye degradation

1 Introduction

Water pollution has been a major issue of concern due to the serious impact on all living creatures [1]. It has already been reported that the major organic compounds, which contribute to environmental danger are the textile as well as other industrial dyes [2]. Many dyes are nontoxic by themselves but when they are mixed with water, they easily form highly toxic complexes in wastewater and this wastewater can pollute water sources if improperly discharged to the environment. To suppress or alleviate the increasingly worsening problem of water contamination, advanced oxidation processes (AOPs) are intensively being developed as innovative water treatment technologies. Among various AOPs, heterogeneous photocatalysis has been shown to have a great potential as a low-cost, environmentally friendly and sustainable treatment technology to tally with the "zero" waste scheme in the water/wastewater industry [3].

The performance of catalysts is a critical factor affecting photocatalytic efficiency. A great number of semiconductor materials have already been tested as photocatalysts to degrade pollutants. The transition metal oxides not only have semiconductor properties, but also have excellent redox properties owing to unfilled valence d-orbitals that lose or seize electrons easily, making them superior metal oxide catalysts. As a II–VI semiconductor with thermal stability, ZnO exhibits sensitive response to both ultraviolet (UV) and visible light [4], and is widely applied in many fields, such as manufacture of lasers and UV light-emitting-diodes. Moreover, in the chemical industry, ZnO is widely used as a heterogeneous catalyst for the production of many chemicals such as methanol [5]. However, the catalytic efficiency of ZnO is restricted by its low adsorption ability, fast electron-hole recombination and limited reusability [6]. Manganese is an active and common metal that is easily oxidized in nature. Due to rich redox and catalytic properties, manganese and different

Received August 4, 2019; accepted October 21, 2019

E-mails: jma@zju.edu.cn (Ma J), sxk7@psu.edu (Komarneni S)

forms of manganese oxides are known to play an important role in catalyzing numerous organic reactions [7,8]. In addition, transition metal composite oxides often have better properties than a single oxide, in the fields such as electronics, optics, and magnetics. Transition metal composite oxides also have good stability, corrosion resistance, high temperature resistance, high hardness and other characteristics. Compared with common single-metal oxides, the spinels AB_2O_4 (A, B = metal) are more attractive by virtue of electron hopping between different valence states of metals in O-sites and also supply necessary surface active metal centers for redox reaction [9–12]. Among the spinels, zinc manganese oxides have attracted much attention owing to their tremendous technological importance as catalyst, solid electrolyte [9,13], and so on. Khaksar et al. [14] synthesized $Zn_{1-x}Mn_xO$ nanoparticles by a polyethylene glycol sol-gel method and applied them as a catalyst along with H_2O_2 as the oxidant to degrade methylene blue completely. Qiu et al. [15] used Fenton-like catalysts and H_2O_2 to degrade methyl violet, and found that the synthesized $ZnMn_2O_4$ nanorod exhibited much better catalytic performance than $ZnMnO_3$ nanorods, because the $t_{2g}^3e_g^1$ electron configuration of Mn(III) in $ZnMn_2O_4$ could facilitate the dissociation of oxygen-containing radicals ($HO^•$ and $HOO^•/O_2^{•-}$). Nevertheless, not much research has been done on the photocatalytic activity of zinc manganese oxides. Borhade et al. [16] used mechanochemical method to prepare the hexagonal nanocrystalline $ZnMnO_3$ powder and found that the $ZnMnO_3$ exhibited a pronounced photocatalytic activity under UV-visible light irradiation and could almost degrade Erioglaucine dye completely. Li and Xu [17] adopted the method composed of electrospinning technique and subsequent calcination to fabricate Zn-Mn-O heterostructures with unique morphologies and applied them in degradation of methylene blue. The results indicated that the catalytic performance of the samples followed the sequence: $ZnMnO_3/ZnMn_2O_4 > ZnO/ZnMnO_3 > ZnMn_2O_4$. It was pointed out that the heterostructures of $ZnMnO_3/ZnMn_2O_4$ with fan-like side morphology had a loose porous surface which facilitated the interaction/reaction between samples and organics, resulting in their higher photocatalytic activity [17].

With further developments of photocatalysis, it has been shown that the addition of small quantities of oxidants such as H_2O_2 leads to an increase in the formation of hydroxyl radicals. The combination of photocatalyst and oxidants has the capability of oxidizing several highly refractory compounds [4]. However, some oxidants such as O_3 and H_2O_2 that are commonly used to produce strongly oxidizing hydroxyl radicals may be limited in application due to cost-intensive production of oxidants, transport and storage of H_2O_2, pH adjustments, and sludge generation [18]. Compared to $HO^•$ (1.8–2.7 V vs NHE, pH dependent), sulfate radical ($SO_4^{•-}$) is a very strong one-electron oxidant (2.5–3.1 V) [19], and is expected to degrade most of the environmentally toxic chemicals in a wide pH range (2.0–8.0) [20]. In addition, on account of the convenience of storage and transport, pH-tolerance and stability [21], sulfate radical-based AOPs are garnering broad attention as one of the most promising ways for the destruction of organic contaminants in water [20,22]. Persulfate (peroxymonosulfate (PMS, HSO_5^-) and peroxydisulfate (PDS, $S_2O_8^{2-}$)) are commonly used as precursors of sulfate radicals and can be activated to generate $SO_4^{•-}$ by using heat [23], UV [23,24], base [25,26], transition metals [27,28], electrochemical means [29,30] or other ways [31,32]. However, intensive energy input, which is required for activation, high costs of oxidants and risks of secondary pollution represent the main practical constraints for persulfate pilot-scale application. Considering the fact that sulfite and bisulfite (BS) may be relatively cheap and easy to obtain and can be finally oxidized to the harmless sulfate ion, it is possible to use sulfite or BS to enhance the degradation of organic contaminants in water [33].

Sun et al. [34,35] studied the activation of manganese oxidants with BS, and proposed the influencing factors and reaction mechanism of permanganate/BS (PM/BS) process. These researchers found that soluble Mn(III) generated in the activation of permanganate/BS could oxidize organic contaminants rapidly and the fraction of Mn(III) effective for decomposing organic contaminant could be decreased by the presence of excessive BS or by the rapid disproportionation of Mn(III) at $pH \geqslant 7.0$ [36]. The PM/BS process may lead to a new category of advanced oxidation technologies based on contaminant oxidation by reactive Mn(III), rather than hydroxyl and sulfate radicals [34].

Herein we report the synthesis of $ZnMn_2O_4$ nanoparticles via a sucrose-aided combustion method and their use as a catalyst to degrade orange II in three different systems, i.e., photocatalysis, chemocatalysis, and photo-chemical catalysis. The influences of material composition, morphology and chemical environment on the degradation process is investigated. Furthermore, the stability and recyclability of the $ZnMn_2O_4$ sample is also investigated.

2 Experimental

2.1 Materials

$Mn(NO_3)_2 \cdot 4H_2O$, sucrose, $NaHSO_3$, MeOH, ethylenediaminetetraacetic acid disodium salt (EDTA-2Na) were supplied by the Shanghai Titan Scientific Co., Ltd. (Shanghai, China). $Zn(NO_3)_2 \cdot 6H_2O$, *tert*-butanol (TBA) and *p*-benzoquinone (BQ) were purchased from the Shanghai Aladdin Bio-Chem Technology Co., Ltd. (Shanghai, China). $NaNO_3$ and orange II sodium salt

were obtained from the Sinopharm Chemical Reagent Co., Ltd. (Shanghai, China). All the chemicals for this study were at least of analytical grade and were used as received. Deionized water was used throughout the experiments.

2.2 Synthesis of $ZnMn_2O_4$

The $ZnMn_2O_4$ sample was prepared by a straightforward sucrose-aided combustion method [37] with the initial formation of Zn/Mn-sucrose composite and subsequent decomposition. Firstly, 1.1156 g $Zn(NO_3)_2 \cdot 6H_2O$, 1.8826 g $Mn(NO_3)_2 \cdot 4H_2O$ and 0.5990 g sucrose were dissolved in a small amount of distilled water under stirring at room temperature. Then, the solution was heated at 120°C for about 20 min under stirring. Upon further heating, the material dried up and started to swell due to the evolution of gases generated during thermolysis of the reagents, resulting in a foamy mass. After a few minutes, the mass started to burn up spontaneously without flame, yielding the precursor Zn/Mn-sucrose composite which was a very light and fluffy black powder. Finally, the obtained composite was heated by a muffle furnace in air at 600°C for 4 h with a heating rate of $5°C \cdot min^{-1}$.

2.3 Characterization

The crystallinity, crystalline phases and phase purity of the catalyst were analyzed by powder X-ray diffraction (XRD) using a Rigaku D/Max-2500 PC X-ray diffractometer with Cu Kα radiation. The morphology of the catalyst was characterized by the JSM-6360LA scanning electron microscope (SEM, JEOL, Japan). The BET specific surface area was recorded on a nitrogen-adsorption system (ASAP 2010C, USA). The distribution of each element was studied by X-ray photoelectron spectroscopy (XPS) performed on a Thermo Scientific, Escalab 250Xi spectrometer with monochromatic Al X-ray source (Al Kα, hν = 1486.7 eV). Ion chromatography (Dionex ICS-1100) was used to detect the sulfite and sulfate ions.

2.4 Catalytic degradation of orange II

The catalytic activities of the as-obtained $ZnMn_2O_4$ sample were tested for the degradation of orange II in three types of systems, i.e., photocatalysis, chemocatalysis and photochemical catalysis which is a combination of the former two systems. The photocatalysis system was used with visible light irradiation, using a home-made photoreactor containing 5 × 24 W LED lamps. The chemocatalysis system was set up in the presence of $NaHSO_3$. The photochemical catalysis system was a combination of both visible light irradiation and sodium BS. All experiments were conducted in a 100 mL vessel containing a solution of orange II (6 ppm) at room temperature. For each experiment, 0.1 g of the as-synthesized $ZnMn_2O_4$ sample was added into the orange II solution and its catalytic performance in different systems was evaluated using various factors. With the continuous magnetic stirring, samples were taken out at regular time intervals from the suspension during the 120-min reaction process. The collected suspensions were centrifuged to filter out the $ZnMn_2O_4$ nanocrystals and then the nanocrystal free solution was analyzed using a UV-Vis spectrophotometer (UV-2450, Shimadzu, Japan).

To examine the stability and recyclability of the $ZnMn_2O_4$ catalyst, recycling experiments were conducted. The used catalyst was collected by filtration after each cycle followed by washing with deionized water and ethanol several times and drying at 60°C overnight. The dose of the catalyst and other reaction conditions remained the same in each run.

3 Results and discussion

3.1 Characterization

The XRD pattern of the $ZnMn_2O_4$ catalyst is shown in Fig. 1. The characteristic diffraction peaks for the sample were detected at 2θ angles of 18.2°, 29.3°, 31.2°, 33.0°, 36.4°, 38.9°, 44.7°, 50.7°, 51.9°, 54.4°, 56.7°, 59.0°, 60.8°, 65.1°, 70.9°, 75.0°, 77.3° and 78.6°, which are consistent with (101), (112), (200), (103), (211), (004), (220), (204), (105), (312), (303), (321), (224), (400), (305), (413), (422) and (404) crystal planes of tetragonal $ZnMn_2O_4$ (JCPDS file No. 77-0470), respectively. No characteristic peak from any impurities could be detected.

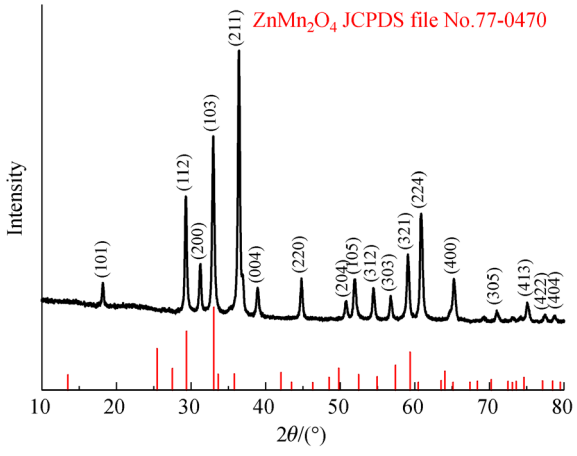

Fig. 1 XRD pattern of the $ZnMn_2O_4$ catalyst.

Typical SEM images of the $ZnMn_2O_4$ catalyst are shown in Fig. 2. The $ZnMn_2O_4$ catalyst exists in the form of nanoparticles of 15–110 nm in size (Figs. 2(a) and 2(b)). At higher magnification (Figs. 2(c) and (d)), some thick, very loose plate-like structures with many macropores on their surfaces were observed. The precursor Zn/Mn-sucrose composite was very fluffy before heating at 600°C and as

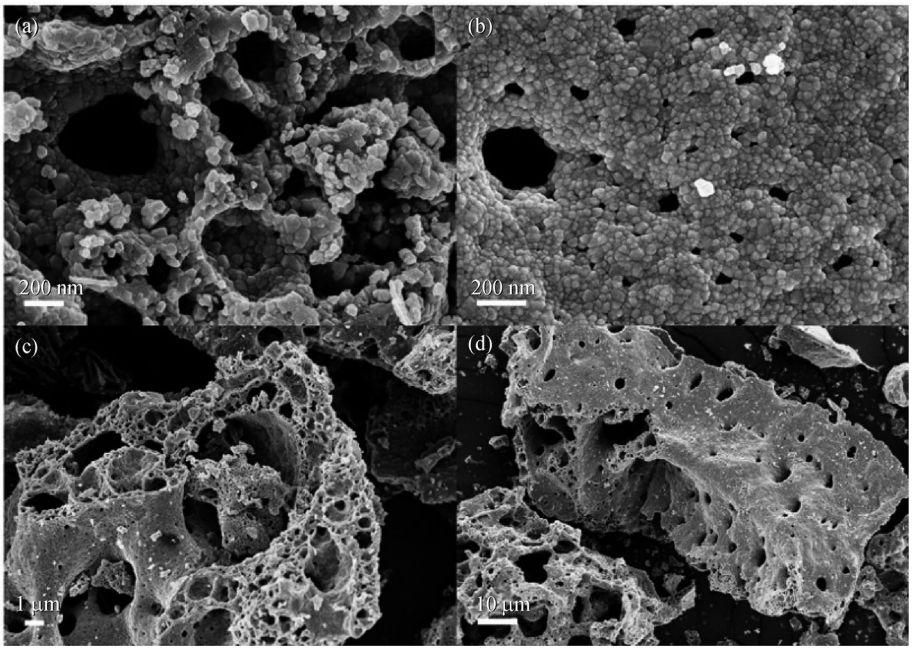

Fig. 2 SEM images of the $ZnMn_2O_4$ catalyst.

the sucrose decomposed during the calcination process, a loose and porous structure of the $ZnMn_2O_4$ catalyst was formed because of the escaping gases.

The $ZnMn_2O_4$ catalyst prepared by the sucrose-aided combustion method, however, has a low surface area of 19.1 $m^2 \cdot g^{-1}$ for the powder annealed at 600°C in air.

3.2 Performance of the $ZnMn_2O_4$ catalyst for orange II degradation

As shown in Fig. 3(a), orange II was used as a model contaminant to evaluate the catalytic activities of the $ZnMn_2O_4$ sample under different conditions. As an anionic azo dye, orange II is refractory with good stability [38]. After 120 min of visible light irradiation, the concentration of the orange II solution hardly changed, suggesting that there is no photobleaching of pure orange II dye. The blank tests showed that in the absence of the catalyst, sodium BS could degrade the dye to some extent (26%), and the degradation efficiency improved to 37% after adding illumination, indicating that some active species were generated in the BS solution. However, more active substances were produced under light irradiation, which increased the degradation efficiency further. Because the degradation experiments were performed in open air, BS could be oxidized by oxygen to produce $SO_4^{\bullet -}$ (Eq. 1) [39]. Then, $HO^{\bullet}$ would appear after $SO_4^{\bullet -}$ reacts with OH^- (Eq. 2) [40]. As a weak electrolyte, HSO_3^- was partially ionized in water to give H^+ and SO_3^{2-}. When HSO_3^- solution is irradiated with light, sulfite radicals ($SO_3^{\bullet -}$) and hydrated electrons (e_{aq}^-) are produced by sulfite photolysis (Eq. 3) [41]. Hydrated electron (e_{aq}^-) is a powerful reducing species which can reduce and decolorize the dye molecule [42].

$$2HSO_3^- + O_2 \rightarrow SO_4^{\bullet -} + SO_4^{2-} + 2H^+ \quad (1)$$

$$SO_4^{\bullet -} + OH^- \rightarrow SO_4^{2-} + HO^{\bullet} \quad (2)$$

$$SO_3^{2-} + h\nu \rightarrow SO_3^{\bullet -} + e_{aq}^- \quad (3)$$

Less than 3% of the dye was adsorbed on $ZnMn_2O_4$ under dark condition and hence, the role of adsorption appears to be very limited. However, the degradation results of orange II with the $ZnMn_2O_4$ catalyst varied widely among different systems. In the photocatalysis system, the orange II removal was about 15% in the presence of the $ZnMn_2O_4$ catalyst alone under visible light irradiation, suggesting that $ZnMn_2O_4$ could be activated by visible light. When the $ZnMn_2O_4$ catalyst interacted with BS, 67% of the dye was destroyed within 120 min in the chemocatalysis system. However, with the $ZnMn_2O_4$/Vis/BS combined system, namely photo-chemical catalysis system, the reaction rate was much faster than the above two cases and a dramatic orange II degradation of 90% was achieved during the experimental period. To investigate the concentration of sulfate ions in the solutions, several solutions after reaction were analyzed by ion chromatography, and deionized water was also applied as the blank group. As shown in Fig. 3(b), the sulfate ion concentration of the deionized water is about 0.66 $mg \cdot L^{-1}$, and the concentration of the orange II solution with BS is 2.84 $mg \cdot L^{-1}$, whereas the sulfate ion concentration is about 4.18 $mg \cdot L^{-1}$ for the solution either in the chemocatalysis

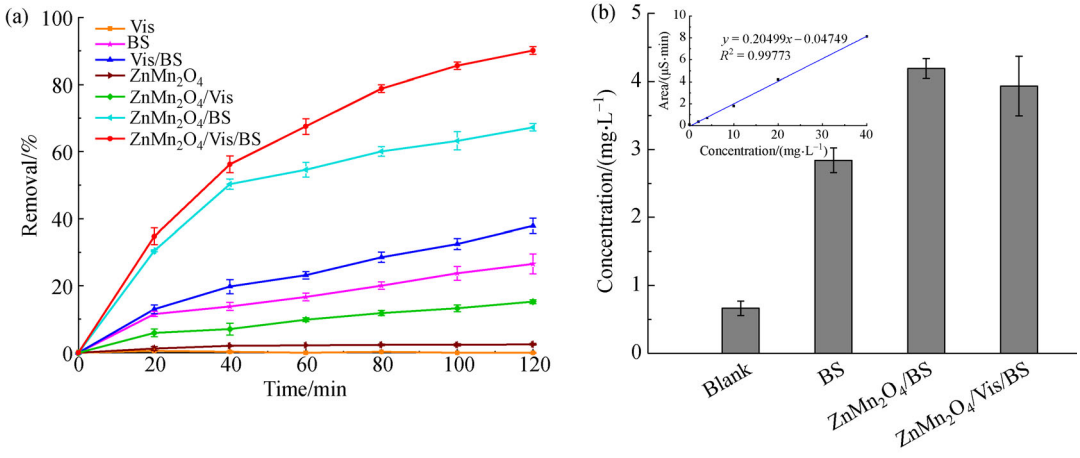

Fig. 3 (a) Orange II degradation in different systems, and (b) sulfate ion concentration in different systems. Conditions: orange II 6 mg·L^{-1}, $ZnMn_2O_4$ 1.0 g·L^{-1}, and $NaHSO_3$ 1.2 g·L^{-1}.

system or the photo-chemical catalysis system, indicating that BS is easily oxidized to sulfate and the $ZnMn_2O_4$ catalyst promotes the transformation. The above result suggests that the combined effect of homogeneous and heterogeneous photocatalytic oxidation induced by BS and $ZnMn_2O_4$, respectively, is responsible for the increased orange II degradation.

3.3 Stability

The recyclability of catalyst is an important factor to estimate stability of the catalyst and long-term use in practical applications. As shown in Fig. 4(a), after three successive degradation cycles of orange II in photo-chemical catalysis system, the used $ZnMn_2O_4$ still shows high activity similar to the fresh material, which degrades nearly 90% dye in 120 min. Furthermore, the XRD patterns of the catalyst after different recycling runs shows no significant change in the structure compared with that of the original catalyst (Fig. 4(b)). These results suggest that the as-synthetized $ZnMn_2O_4$ sample is a green and eximious catalyst with high stability and excellent recyclability, which are propitious for the potential environmental applications.

3.4 Mechanisms of degradation

3.4.1 Photocatalysis mechanism

In the photocatalysis system, only 15% orange II is removed through the activation of the $ZnMn_2O_4$ catalyst by visible light, possibly due to the relatively small active surface. According to the photocatalysis mechanism, when a photon with energy greater than or equal to the bandgap energy of $ZnMn_2O_4$ is illuminated onto the surface of $ZnMn_2O_4$, the lone electron is photoexcited to the empty conduction band in femtoseconds. The photonic excitation generates an empty unfilled valence band and the electron-hole pair (Eq. 4) [43]. The holes can remove orange II by direct oxidation or formation of HO$^{\bullet}$ via the reaction with

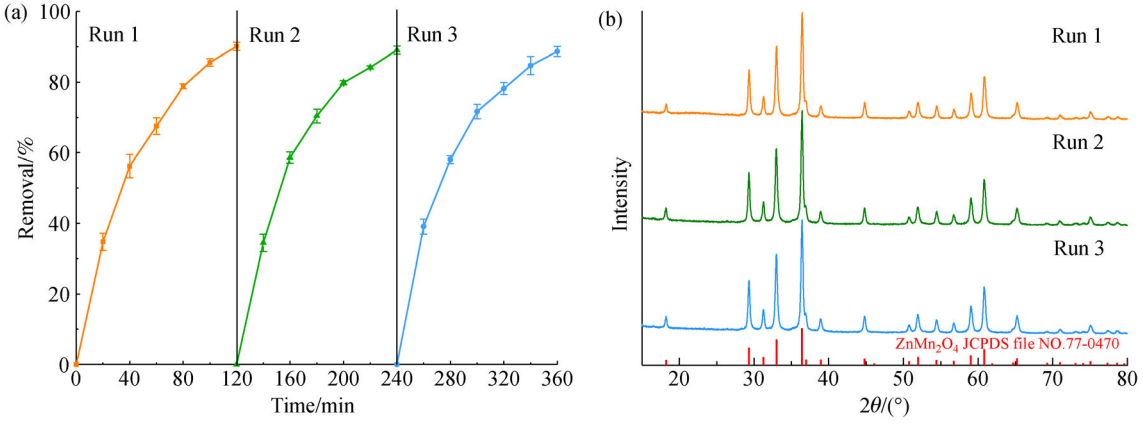

Fig. 4 (a) Recycling runs for the degradation of orange II in the photo-chemical catalysis system (Conditions: orange II 6 mg·L^{-1}, $ZnMn_2O_4$ 1.0 g·L^{-1}, and $NaHSO_3$ 1.2 g·L^{-1}); (b) XRD patterns of the $ZnMn_2O_4$ after different recycling runs.

the surface-adsorbed OH groups (Eqs. 5 and 7) [38]. Moreover, radiolysis in aqueous solutions causes the charged species to become hydrated within a very short interval of time ([44]. Then, the hydrated electrons are captured by O_2 to form the superoxide radicals ($O_2^{\bullet-}$) (Eq. 6) [42,45], which can also degrade the dye (Eq. 7). Unfortunately, it is difficult to effectively utilize the photo-generated electron–holes because of their rapid recombination. Therefore, the photocatalytic activity is relatively low in the $ZnMn_2O_4$/Vis system.

$$\text{catalyst} + h\nu \rightarrow e^- + h^+ \quad (4)$$

$$h^+ + OH^- \rightarrow HO^\bullet \quad (5)$$

$$e_{aq}^- + O_2 \rightarrow O_2^{\bullet-} \quad (6)$$

$$h^+/O_2^{\bullet-}/HO^\bullet/e_{aq}^- + \text{dyes} \rightarrow \text{products} \quad (7)$$

3.4.2 Chemocatalysis mechanism

In the chemocatalysis system, the $ZnMn_2O_4$ sample was used as the catalyst and BS was used as the oxidant to degrade orange II under the dark condition. The degradation process was monitored by UV-visible spectrometry to verify the fast-chemical destruction of azo bond in orange II. As shown in Fig. 5, the intense absorbance of orange II at wavelength of 484 nm decreases rapidly in the first 40 min and eventually to 33% of the initial value after 120 min. In the presence of BS, the $ZnMn_2O_4$ catalyst shows a good catalytic ability, indicating that the $ZnMn_2O_4$ catalyst is activated by BS and some active species produced during the process are propitious for degradation. Driven by the $ZnMn_2O_4$ catalyst, BS is oxidized to $SO_3^{\bullet-}$ (Eq. 8) [46]. Under aerobic atmosphere, the generated $SO_3^{\bullet-}$ rapidly reacts with oxygen and gave rise to the formation of the oxygen-centered PMS ($SO_5^{\bullet-}$) and sulfate ($SO_4^{\bullet-}$) anion radicals through subsequent reactions (Eqs. 9 and 10) [47]. As described in Eq. 2, hydroxyl radicals are produced from the redox reaction between $SO_4^{\bullet-}$ and OH^-. As highly reactive radicals, both $HO^\bullet$ and $SO_4^{\bullet-}$ accelerate the breakdown of the dye (Eq. 11).

To cast more light on the reaction mechanism, the relative contributions of the active species mentioned above should be assessed by adding corresponding radical scavengers. Therefore, TBA was selected as the $HO^\bullet$ scavenger because it has high reactivity toward $HO^\bullet$ (k = 6.0×10^8 L·mol^{-1}·s^{-1}) and much lower reactivity toward $SO_4^{\bullet-}$ (k = 8.0×10^5 L·mol^{-1}·s^{-1}) [48], whereas MeOH was chosen as an effective quencher for both $SO_4^{\bullet-}$ and $HO^\bullet$ due to its high rate constants with $SO_4^{\bullet-}$ ($k = 2.5 \times 10^7$ L·mol^{-1}·s^{-1}) and $HO^\bullet$ (k = 9.7×10^8 L·mol^{-1}·s^{-1}). Furthermore, $SO_3^{\bullet-}$ and $SO_5^{\bullet-}$ are relatively inert to alcohols. As shown in Fig. 6, after adding TBA, the degradation rate of orange II is reduced to 20%, and even lower in the presence of MeOH. However, the inhibition of TBA is more significant, so $HO^\bullet$ is the main active substance in the chemocatalysis system.

$$\text{catalyst} + HSO_3^- \rightarrow SO_3^{\bullet-} \quad (8)$$

$$SO_3^{\bullet-} + O_2 \rightarrow SO_5^{\bullet-} \quad (9)$$

$$SO_5^{\bullet-} + SO_3^{2-} \rightarrow SO_4^{\bullet-} + SO_4^{2-} \quad (10)$$

$$HO^\bullet/SO_4^{\bullet-} + \text{dyes} \rightarrow \text{products} \quad (11)$$

3.4.3 Photo-chemical catalysis mechanism

In the photo-chemical catalysis system, where both visible light irradiation and BS were present, the $ZnMn_2O_4$ sample exhibited excellent catalytic capability. Representative

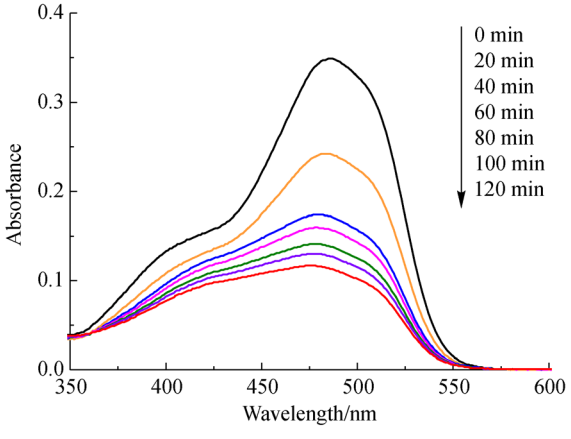

Fig. 5 UV-Vis spectra during the degradation of orange II for the chemocatalysis system. Conditions: orange II 6 mg·L^{-1}, $ZnMn_2O_4$ 1.0 g·L^{-1}, and $NaHSO_3$ 1.2 g·L^{-1}

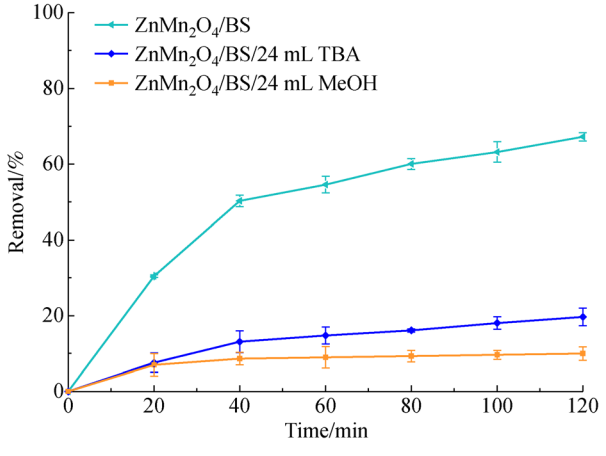

Fig. 6 Orange II degradation in the chemocatalysis system. Conditions: orange II 6 mg·L^{-1}, $ZnMn_2O_4$ 1.0 g·L^{-1}, and $NaHSO_3$ 1.2 g·L^{-1}.

changes in UV-Vis spectra during orange II decolorization in the photo-chemical catalysis system are depicted in Fig. 7. The main absorption band at 484 nm drastically diminishes within 120 min, indicating almost complete destruction of the dye. The removal of orange II in the photo-chemical catalysis system is 90%, which is much higher than that in the photocatalysis system (15%) and higher than that in the chemocatalysis system (67%). This result indicates that the $ZnMn_2O_4$ catalyst is activated by BS and visible light, and they interact with each other to produce some unique active species, rather than due to a simple addition of the respective effects.

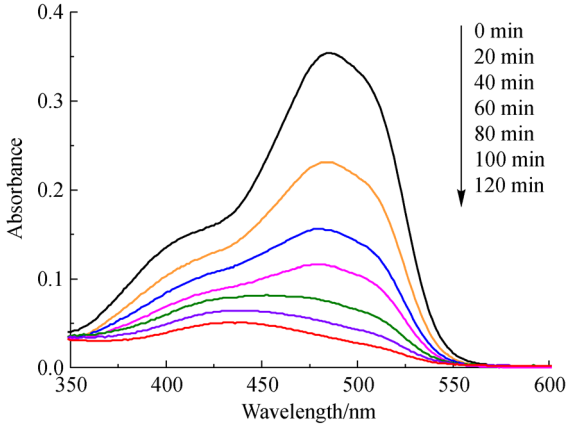

Fig. 7 UV-Vis spectra during the degradation of orange II for the photo-chemical catalysis system. Conditions: orange II 6 mg·L^{-1}, $ZnMn_2O_4$ 1.0 g·L^{-1}, and $NaHSO_3$ 1.2 g·L^{-1}.

To further understand the confinement and synergistic effects of $ZnMn_2O_4$ catalyst in the heterogeneous reaction, XPS was applied to evaluate the chemical composition of active species for the fresh and used $ZnMn_2O_4$. The survey spectrum indicates the presence of Mn, Zn, O and C elements on the catalyst surface (Fig. 8(a)). Owing to hydrocarbon contaminants, small amount of C is present in the XPS spectra, which is a common feature of XPS analysis. The high resolution spectrum of each element is corrected using the standard correction factor C 1s (284.8 eV). In Fig. 8(b), the Mn 2p spectra featured two strong spin-orbital peaks of Mn $2p_{3/2}$ centered at 641.8 eV and Mn $2p_{1/2}$ at 653.7 eV. Gaussian-Lorentzian curve fitting of Mn $2p_{3/2}$ and Mn $2p_{1/2}$ was carried out to describe the oxidation states of the $ZnMn_2O_4$ catalyst. For Mn $2p_{3/2}$, two peaks at 641.4 and 642.8 eV were obtained, which can be assigned to Mn(II) and Mn(III) oxidation states with a ratio of 0.35:0.65. After the reaction, the area ratio of Mn(II)/Mn(III) is changed to a lower value of 0.25:0.75. The obvious change of Mn valence indicates that Mn species on catalyst surface participate in the heterogeneous catalytic reaction. Mn(II) provides electrons and partially contributes to the increase of Mn(III). For the XPS spectrum of Zn shown in Fig. 8(c), the binding energies at 1021.4 and 1044.5 eV for $2p_{3/2}$ and $2p_{1/2}$ correspond to Zn(II) states, and the Zn $2p_{3/2}$ spectrum of Zn oxide is free from multiplet splitting and other complicating effects. In the case of O 1s spectra (Fig. 8(d)), two oxygen species can be seen, i.e., the surface lattice oxygen species (O_{latt}) at 529.9 eV, which is the dominant component of the catalysts, and the surface adsorbed oxygen species (O_{ads}) at 531.1 eV that could be the most active oxygen species during the surface catalytic reaction. Compared with the ratio of the peak area before reaction, the relative content of O_{latt} is reduced from 60% to 49% after the reaction, whereas O_{ads} content increases from 40% to 51%. The increased ratio of O_{ads} is ascribed to the formation of M-OH (M = Mn or Zn) groups or O^{2-} adsorbed on the catalyst surface. From the above analysis, the $ZnMn_2O_4$ catalyst appears to experience an oxidation process and thus, leading to increased relative contents of Mn(III) and O_{ads} found on the surface of catalyst.

As described in the chemocatalysis system, when the catalyst reacts with BS, BS is oxidized to $SO_3^{\bullet-}$ and converted to $SO_4^{\bullet-}$ through a series of reactions (Eqs. 8 to 10), whereas Mn(III) on the surface of the catalyst is reduced to Mn(II) (Eq. 12) [46]. Mn(II) is supposed to change to Mn(III) after trapping holes generated under illumination (Eq. 13) [49] but quickly return to Mn(II) after oxidizing OH^- is adsorbed on the surface to form $HO^{\bullet}$ (Eq. 14) [50]. Such shallow trapping could thus separate e^-/h^+ pairs at the surface to greatly reduce their recombination on the surface of $ZnMn_2O_4$, making some contribution to the superior degradation effect in the photo-chemical catalysis system. As a strong and important oxidant for one electron transfer reactions, Mn(III) could rapidly degrade the organic contaminants and promote the reaction process (Eq. 15) [34]. Furthermore, $O_2^{\bullet-}$, h^+, $SO_4^{\bullet-}$, $HO^{\bullet}$ and other active species generated in the reaction also contribute to the ultimate efficient degradation (Eq. 16).

$$\mathrm{Mn(III) + HSO_3^- \rightarrow Mn(II) + SO_3^{\bullet-} + H^+} \quad (12)$$

$$\mathrm{Mn(II) + h^+ \rightarrow Mn(III)} \quad (13)$$

$$\mathrm{Mn(III) + OH^- \rightarrow Mn(II) + HO^{\bullet}} \quad (14)$$

$$\mathrm{Mn(III) + dyes \rightarrow Mn(II) + products} \quad (15)$$

$$\mathrm{O_2^{\bullet-}/h^+/SO_3^{\bullet-}/HO^{\bullet}/e_{aq}^- + dyes \rightarrow products} \quad (16)$$

To delve into the contributions of some possible active species involved in the photo-chemical degradation process, scavenging experiments of hydrated electrons, holes, superoxide radicals, hydroxyl radicals and sulfate radicals were conducted. Figure 9 shows the inhibition effects of the corresponding scavengers on the degradation

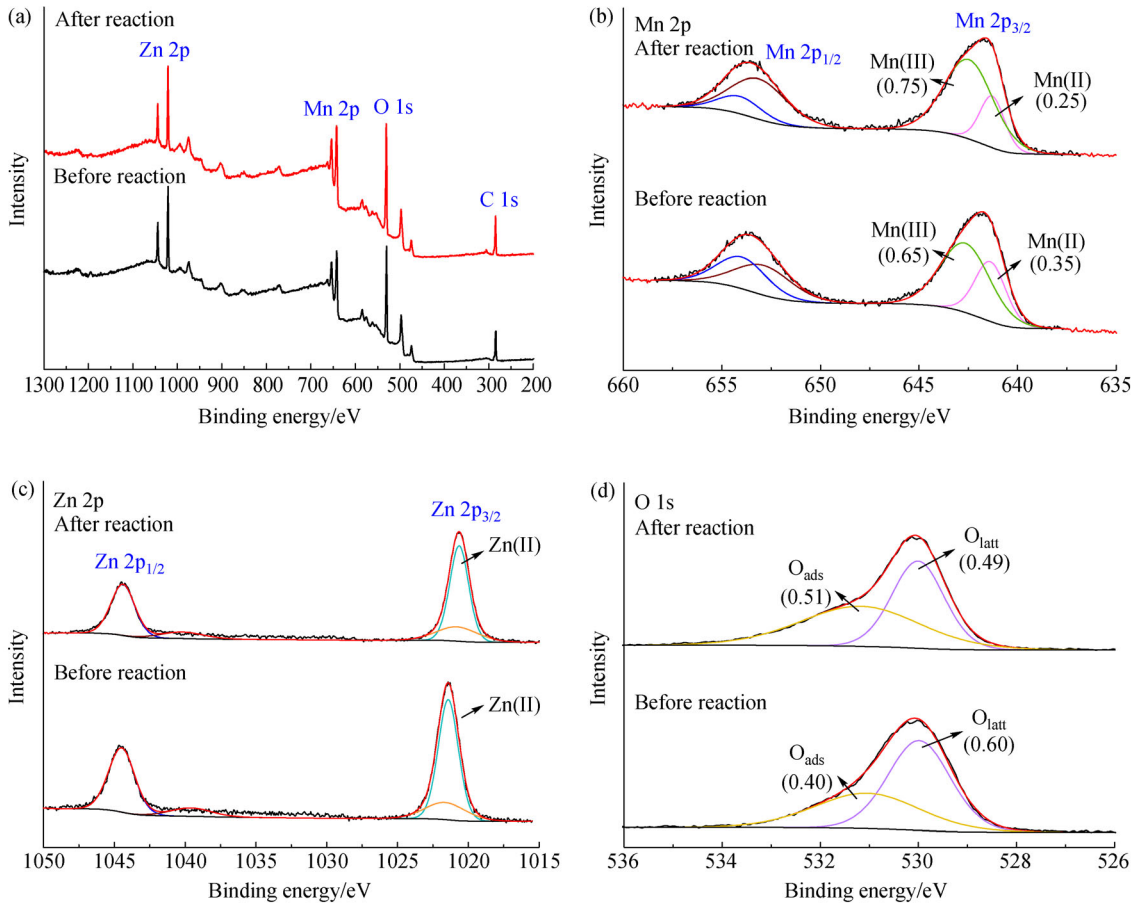

Fig. 8 XPS spectra of $ZnMn_2O_4$ catalyst before and after reaction: (a) survey, (b) Mn 2p, (c) Zn 2p, and (d) O 1s.

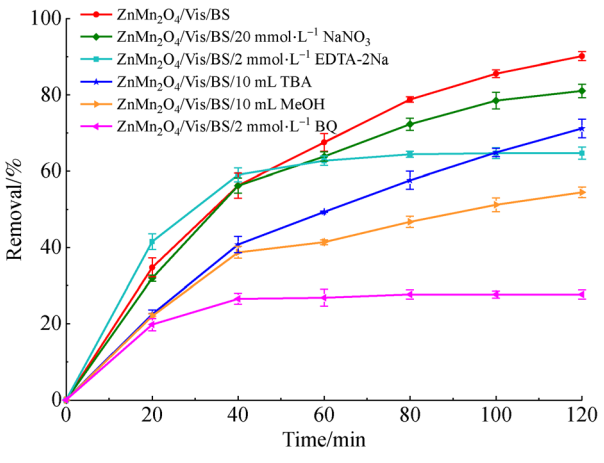

Fig. 9 Orange II degradation in the photo-chemical catalysis system. Conditions: orange II 6 mg·L^{-1}, $ZnMn_2O_4$ 1.0 g·L^{-1}, and $NaHSO_3$ 1.2 g·L^{-1}.

of orange II in the $ZnMn_2O_4$ catalyst/Vis/BS system. As a scavenger for hydrated electrons, 20 mmol·L^{-1} nitrate was added into the solution; when compared to the efficiency without scavenger (90%), its inhibition effect is negligible, suggesting that the reaction between e_{aq}^- and orange II might occur to a small extent in the photo-chemical catalysis system. Moreover, the possibility of superoxide radicals reacting with orange II was studied using BQ as a superoxide radical scavenger. Figure 9 shows that the addition of 2 mmol·L^{-1} BQ has significant effect on orange II photo-chemical degradation compared to that without BQ. This result implies that $O_2^{\bullet-}$ makes a substantial contribution to the BS-assisted enhancement in photo-catalysis. According to Eq. 6, $O_2^{\bullet-}$ is formed through the capture of e_{aq}^- by O_2. However, the reaction rate of e_{aq}^- with O_2 ($k = 1.8 \times 10^{10}$ L·mol^{-1}·s^{-1}) [51] is higher than that of e_{aq}^- with nitrate ($k = 9.7 \times 10^9$ L·mol^{-1}·s^{-1}) [41]. Therefore, most of e_{aq}^- in the relaction is captured to form $O_2^{\bullet-}$, leading to a large amount of $O_2^{\bullet-}$ and a small amount of e_{aq}^- in the solution, which is consistent with the experimental results that BQ could inhibit 63% degradation while nitrate could only inhibit 9%. Besides, after adding 2 mmol·L^{-1} EDTA-2Na to quench the effect of holes, the removal rate of orange II is reduced to 64%. This result confirms that h^+ plays a role in the degradation process, including assisting in the generation of $HO^{\bullet}$ and

reacting directly with the dye. However, the addition of TBA reduces the degradation rate to 71%; this suppressive effect is slightly lower than that of EDTA-2Na, because TBA only captures $HO^{\bullet}$ in the process, while the holes on the catalyst surface still survive to further generate free radicals. When MeOH is included in the reaction, only 54% of the dye is removed, indicating that $HO^{\bullet}$ and $SO_4^{\bullet-}$ are involved in the reaction at the same time. These experimental results confirm the existence and promoting effects of $O_2^{\bullet-}$, h^+, $SO_4^{\bullet-}$, $HO^{\bullet}$ and e_{aq}^- species in the orange II degradation process.

4 Conclusions

A $ZnMn_2O_4$ catalyst has been prepared by a sucrose-aided combustion method. It can be activated by visible light irradiation (photocatalysis sytem) or BS (chemocatalysis system) to degrade orange II but the removal rate of orange II is the highest (90%) in the photo-chemical catalysis system where visible light and BS coexist. Recycling experiments confirm that the $ZnMn_2O_4$ catalyst has excellent stability and recyclability. Based on the results of characterization and radical scavenging experiments, the rational degradation mechanisms of the three different catalytic systems are proposed. Some active species such as Mn(III), $O_2^{\bullet-}$, h^+, e_{aq}^-, $SO_4^{\bullet-}$ and $HO^{\bullet}$ may be responsible for the degradation acceleration of orange II.

Acknowledgements This work was supported by the National Natural Science Foundation of China (Grant No. 21477009), Natural Science Foundation of Jiangsu Province (No. SBK2016021419), "333 project" of Jiangsu Province and the Opening Project of Guangxi Key Laboratory of Green Processing of Sugar Resources (No. GXTZY201803). One of us (SK) was supported by the College of Agricultural Sciences under Station Research Project No. PEN04566.

References

1. Gupta V K, Ali I, Saleh T A, Nayak A, Agarwal S. Chemical treatment technologies for waste-water recycling: An overview. RSC Advances, 2012, 2(16): 6380–6388
2. Li J P, Xu Y, Liu Y, Wu D, Sun Y H. Synthesis of hydrophilic ZnS nanocrystals and their application in photocatalytic degradation of dye pollutants. China Particuology, 2004, 2(6): 266–269
3. Chong M N, Jin B, Chow C W K, Saint C. Recent developments in photocatalytic water treatment technology: A review. Water Research, 2010, 44(10): 2997–3027
4. Shukla P R, Wang S, Ang H M, Tadé M O. Photocatalytic oxidation of phenolic compounds using zinc oxide and sulphate radicals under artificial solar light. Separation and Purification Technology, 2010, 70(3): 338–344
5. Ludi B, Niederberger M. Zinc oxide nanoparticles: Chemical mechanisms and classical and non-classical crystallization. Dalton Transactions (Cambridge, England), 2013, 42(35): 12554–12568
6. Liu S W, Li C, Yu J G, Xiang Q J. Improved visible-light photocatalytic activity of porous carbon self-doped ZnO nanosheet-assembled flowers. CrystEngComm, 2011, 13(7): 2533–2541
7. Duan L, Sun B, Wei M, Luo S, Pan F, Xu A, Li X. Catalytic degradation of acid orange 7 by manganese oxide octahedral molecular sieves with peroxymonosulfate under visible light irradiation. Journal of Hazardous Materials, 2015, 285: 356–365
8. Hocking R K, Brimblecombe R, Chang L Y, Singh A, Cheah M H, Glover C, Casey W H, Spiccia L. Water-oxidation catalysis by manganese in a geochemical-like cycle. Nature Chemistry, 2011, 3 (6): 461–466
9. Zhang L, Yang C, Xie Z, Wang X. Cobalt manganese spinel as an effective cocatalyst for photocatalytic water oxidation. Applied Catalysis B: Environmental, 2018, 224: 886–894
10. Cheng F, Shen J, Peng B, Pan Y, Tao Z, Chen J. Rapid room-temperature synthesis of nanocrystalline spinels as oxygen reduction and evolution electrocatalysts. Nature Chemistry, 2011, 3(1): 79–84
11. Menaka, Samal S L, Ramanujachary K V, Lofland S E, Govind, Ganguli A K. Stabilization of Mn(IV) in nanostructured zinc manganese oxide and their facile transformation from nanospheres to nanorods. Journal of Materials Chemistry, 2011, 21(24): 8566–8573
12. Cady C W, Gardner G, Maron Z O, Retuerto M, Go Y B, Segan S, Greenblatt M, Dismukes G C. Tuning the electrocatalytic water oxidation properties of AB_2O_4 spinel nanocrystals: A (Li, Mg, Zn) and B (Mn, Co) site variants of $LiMn_2O_4$. ACS Catalysis, 2015, 5 (6): 3403–3410
13. Cui B, Lin H, Liu Y Z, Li J B, Sun P, Zhao X C, Liu C J. Photophysical and photocatalytic properties of core-ring structured $NiCo_2O_4$ nanoplatelets. Journal of Physical Chemistry C, 2009, 113 (32): 14083–14087
14. Khaksar M, Amini M, Boghaei D M. Efficient and green oxidative degradation of methylene blue using Mn-doped ZnO nanoparticles ($Zn_{1-x}Mn_xO$). Journal of Experimental Nanoscience, 2015, 10(16): 1256–1268
15. Qiu M, Chen Z, Yang Z, Li W, Tian Y, Zhang W, Xu Y, Cheng H. $ZnMn_2O_4$ nanorods: An effective Fenton-like heterogeneous catalyst with $t_{2g}^3e_g^1$ electronic configuration. Catalysis Science & Technology, 2018, 8(10): 2557–2566
16. Borhade A V, Tope D R, Dabhade G B. Removal of erioglaucine dye from aqueous medium using ecofriendly synthesized $ZnMnO_3$ photocatalyst. e-Journal of Surface Science and Nanotechnology, 2017, 15: 74–80
17. Li C J, Xu G R. Zn-Mn-O heterostructures: Study on preparation, magnetic and photocatalytic properties. Materials Science and Engineering B, 2011, 176(7): 552–558
18. Yuan S, Fan Y, Zhang Y, Tong M, Liao P. Pd-catalytic *in situ* generation of H_2O_2 from H_2 and O_2 produced by water electrolysis for the efficient electro-fenton degradation of rhodamine B. Environmental Science & Technology, 2011, 45(19): 8514–8520
19. Sun H, Liu S Z, Zhou G, Ang M, Tade M, Wang S. Reduced graphene oxide for catalytic oxidation of aqueous organic pollutants. ACS Applied Materials & Interfaces, 2012, 4(10): 5466–5471
20. Guo Y, Lou X, Fang C, Xiao D, Wang Z, Liu J. Novel photo-sulfite

system: Toward simultaneous transformations of inorganic and organic pollutants. Environmental Science & Technology, 2013, 47 (19): 11174–11181

21. Zhang B T, Zhang Y, Teng Y, Fan M. Sulfate radical and its application in decontamination technologies. Critical Reviews in Environmental Science and Technology, 2015, 45(16): 1756–1800
22. Anipsitakis G P, Dionysiou D D. Degradation of organic contaminants in water with sulfate radicals generated by the conjunction of peroxymonosulfate with cobalt. Environmental Science & Technology, 2003, 37(20): 4790–4797
23. Antoniou M G, de la Cruz A A, Dionysiou D D. Degradation of microcystin-LR using sulfate radicals generated through photolysis, thermolysis and e-transfer mechanisms. Applied Catalysis B: Environmental, 2010, 96(3): 290–298
24. Tan C, Gao N, Deng Y, Zhang Y, Sui M, Deng J, Zhou S. Degradation of antipyrine by UV, UV/H_2O_2 and UV/PS. Journal of Hazardous Materials, 2013, 260: 1008–1016
25. Qi C, Liu X, Ma J, Lin C, Li X, Zhang H. Activation of peroxymonosulfate by base: Implications for the degradation of organic pollutants. Chemosphere, 2016, 151: 280–288
26. Furman O S, Teel A L, Watts R J. Mechanism of base activation of persulfate. Environmental Science & Technology, 2010, 44(16): 6423–6428
27. Yang Q, Choi H, Al-Abed S R, Dionysiou D D. Iron-cobalt mixed oxide nanocatalysts: Heterogeneous peroxymonosulfate activation, cobalt leaching, and ferromagnetic properties for environmental applications. Applied Catalysis B: Environmental, 2009, 88(3-4): 462–469
28. Chen X, Chen J, Qiao X, Wang D, Cai X. Performance of nano-Co_3O_4/peroxymonosulfate system : Kinetics and mechanism study using acid orange 7 as a model compound. Applied Catalysis B: Environmental, 2008, 80(1-2): 116–121
29. Govindan K, Raja M, Noel M, James E J. Degradation of pentachlorophenol by hydroxyl radicals and sulfate radicals using electrochemical activation of peroxomonosulfate, peroxodisulfate and hydrogen peroxide. Journal of Hazardous Materials, 2014, 272 (4): 42–51
30. Jie W, Hui Z, Qiu J. Degradation of acid orange 7 in aqueous solution by a novel electro/Fe^{2+}/peroxydisulfate process. Journal of Hazardous Materials, 2012, 215-216(4): 138–145
31. Liu X, Zhang X, Zhang K, Qi C. Sodium persulfate-assisted mechanochemical degradation of tetrabromobisphenol A: Efficacy, products and pathway. Chemosphere, 2016, 150: 551–558
32. Yan X, Liu X, Qi C, Wang D, Lin C. Mechanochemical destruction of a chlorinated polyfluorinated ether sulfonate (F-53B, a PFOS alternative) assisted by sodium persulfate. RSC Advances, 2015, 5 (104): 85785–85790
33. Qi C, Liu X, Li Y, Lin C, Ma J, Li X, Zhang H. Enhanced degradation of organic contaminants in water by peroxydisulfate coupled with bisulfite. Journal of Hazardous Materials, 2017, 328 (Complete): 98–107
34. Sun B, Guan X, Fang J, Tratnyek P G. Activation of manganese oxidants with bisulfite for enhanced oxidation of organic contaminants: The involvement of Mn(III). Environmental Science & Technology, 2015, 49(20): 12414–12421
35. Sun B, Li D, Linghu W, Guan X. Degradation of ciprofloxacin by manganese(III) intermediate: Insight into the potential application of permanganate/bisulfite process. Chemical Engineering Journal, 2018, 339: 144–152
36. Sun B, Dong H, He D, Rao D, Guan X. Modeling the kinetics of contaminants oxidation and the generation of manganese(III) in the permanganate/bisulfite process. Environmental Science & Technology, 2016, 50(3): 1473–1482
37. Zhao C, Hu Z, Teng Z, Liu K, Zhao D. Porous $ZnMnO_3$ plates prepared from Zn/Mn-sucrose composite as high-performance lithium-ion battery anodes. Micro & Nano Letters, 2016, 11(9): 494–497
38. Cai C, Zhang Z, Liu J, Shan N, Zhang H, Dionysiou D D. Visible light-assisted heterogeneous Fenton with $ZnFe_2O_4$ for the degradation of orange II in water. Applied Catalysis B: Environmental, 2016, 182: 456–468
39. Ni Q, Ma J, Fan C, Kong Y, Peng M, Komarneni S. Spinel-type cobalt-manganese oxide catalyst for degradation of orange II using a novel heterogeneous photo-chemical catalysis system. Ceramics International, 2018, 44(16): 19474–19480
40. Oh W D, Dong Z, Lim T T. Generation of sulfate radical through heterogeneous catalysis for organic contaminants removal: Current development, challenges and prospects. Applied Catalysis B: Environmental, 2016, 194: 169–201
41. Xie B, Li X, Huang X, Xu Z, Zhang W, Pan B. Enhanced debromination of 4-bromophenol by the UV/sulfite process: Efficiency and mechanism. Journal of Environmental Sciences (China), 2017, 54(4): 231–238
42. Ma H, Wang M, Yang R, Wang W, Zhao J, Shen Z, Yao S. Radiation degradation of Congo red in aqueous solution. Chemosphere, 2007, 68(6): 1098–1104
43. Xu T, Zhu R, Zhu G, Zhu J, Liang X, Zhu Y, He H. Mechanisms for the enhanced photo-Fenton activity of ferrihydrite modified with $BiVO_4$ at neutral pH. Applied Catalysis B: Environmental, 2017, 212: 50–58
44. Rauf M A, Ashraf S S. Radiation induced degradation of dyes-An overview. Journal of Hazardous Materials, 2009, 166(1): 6–16
45. Xu T, Zhu R, Zhu J, Liang X, Liu Y, Xu Y, He H. Ag_3PO_4 immobilized on hydroxy-metal pillared montmorillonite for the visible light driven degradation of acid red 18. Catalysis Science & Technology, 2016, 6(12): 4116–4123
46. Sun S, Pang S, Jiang J, Ma J, Huang Z, Zhang J, Liu Y, Xu C, Liu Q, Yuan Y. The combination of ferrate(VI) and sulfite as a novel advanced oxidation process for enhanced degradation of organic contaminants. Chemical Engineering Journal, 2018, 333: 11–19
47. Ranguelova K, Rice A B, Khajo A, Triquigneaux M, Garantziotis S, Magliozzo R S, Mason R P. Formation of reactive sulfite-derived free radicals by the activation of human neutrophils: An ESR study. Free Radical Biology & Medicine, 2012, 52(8): 1264–1271
48. Zou J, Ma J, Chen L W, Li X C, Guan Y H, Xie P C, Pan C. Rapid acceleration of ferrous iron/peroxymonosulfate oxidation of organic pollutants by promoting Fe(III)/Fe(II) cycle with hydroxylamine. Environmental Science & Technology, 2013, 47(20): 11685–11691
49. Liu M, Du Y, Ma L, Jing D, Guo L. Manganese doped cadmium

sulfide nanocrystal for hydrogen production from water under visible light. International Journal of Hydrogen Energy, 2012, 37(1): 730–736

50. Paul S, Chetri P, Choudhury A. Effect of manganese doping on the optical property and photocatalytic activity of nanocrystalline titania: Experimental and theoretical investigation. Journal of Alloys and Compounds, 2014, 583: 578–586
51. Mezyk S P, Neubauer T J, Cooper W J, Peller J R. Free-radical-induced oxidative and reductive degradation of sulfa drugs in water: absolute kinetics and efficiencies of hydroxyl radical and hydrated electron reactions. Journal of Physical Chemistry A, 2007, 111(37): 9019–9024